Effective core polarizabilities in Ba high-l $Nsnl$ double Rydberg atoms

P. Camus and S. Cohen*
Laboratoire Aimé Cotton, Centre National de la Recherche Scientifique II, Bâtiment 505, Campus d'Orsay, 91405 Orsay CEDEX, France
(Received 18 April 1994)

We present experimental energy-level positions for Ba high-l $Nsnl$ double Rydberg states with $N=8$ ($n=13-15$, $l\geq 7$) and $N=9$ ($n=13-15$, $l\geq 7$). These data as well as previously reported measurements for $N=7$ ($n=12-15$, $l\geq 5$) and $N=10$ ($n=13-15$, $l\geq 10$) are parametrized in order to yield values for the Ba^+ Ns effective dipole α_d' and quadrupole α_q' polarizabilities. The obtained α_d' values are $1.25(5)\times 10^3$, $7.05(4)\times 10^3$, $2.95(4)\times 10^4$, $9.39(15)\times 10^4$ in a_0^3 units and the α_q' values are $1.7(8)\times 10^4$, $1.8(2)\times 10^5$, $-1.0(2)\times 10^6$, $-1.0(2)\times 10^7$ in a_0^5 units for $N=7$, 8, 9, and 10, respectively. The α_d' evolution with N is found to follow a $N^{*6.9(1)}$ power law, while calculated static polarizabilities present somewhat lower power dependence. From this small difference it is not possible to appreciate the importance of nonadiabatic effects between the two asymmetrically excited electrons. On the other hand, the larger discrepancies appearing between the calculated static and fitted quadrupole polarizabilities show clear evidence of nonadiabatic effects. Particularly the negative α_q' sign for $N\geq 9$ is attributed to the increasing strength of dynamical effects on the Ns core electron caused by the motion of the outer high-l electron. It gives evidence of the increasing importance of nonadiabatic radial correlation between two planetary electons when the Ns inner electron is sufficiently radially extended to be characterized as an inner Rydberg electron without, nevertheless, any appreciable overlapping with the outer electron.

PACS number(s): 31.25.Jf, 32.10.Dk, 31.50.+w

I. INTRODUCTION

The fundamental three-body Coulomb problem is of long-standing interest in atomic physics. The main reason for this is that the Hamiltonian of the system is in general nonseparable. However, for atomic states with two highly and asymmetrically excited electrons (the outer being in a high-l orbital), several simplifications due to their distinguishability in space and their negligible exchange effects make the problem theoretically tractable. Moreover, these asymmetrical double Rydberg (ADR) states in alkaline-earth atoms (Sr and Ba) are presently investigated experimentally because these possess low-energy double-ionization limits compatible with current laser spectroscopic techniques. Alkaline-earth atoms are considered as the best three-body system simulators in spite of their non-Coulombic doubly charged residual core.

High-l ADR state production is based in a sequential multiphoton or multistep laser excitation of the two valence electrons. The method employs the Stark switching technique, first exciting one valence electron to a high-nl Rydberg state, where it remains inert to further optical excitation, and then exciting the second valence electron in a less radially extended Nl_1 state of the residual singly charged ion. During this latter excitation step, generally described by the isolated core excitation (ICE) formalism, the outer Rydberg electron in the final state reflects the core changes. Moreover, since the centrifugal barrier experienced by the outer electron prevents its penetration to the inner electron as well as the residual doubly charged core, autoionization widths are usually small enough to permit full benefit of the high laser resolution. This allows the observation of spectroscopic events due to the Coulombic repulsion between the two excited electrons.

Experiments performed in high-l $6p_{3/2}nl$, $6d_{5/2}nl$ [1] and $7d_{5/2}nl$ [2] states at $n\approx 11-15$ values revealed the so-called K structures characterizing the onset of long-range correlation between the two excited electrons mainly due to the dipolar term of the Coulombic electron-electron interaction. In another study in Sr [3] the correlation manifestations appear as a mixing with $6gn'l'$ series in the spectra, indicating a strong dipolar polarization of the normally prepared $6f$ inner-electron state in the ICE model.

Recent investigations in Ba $8sn=13l=12-6$ and $n=14l=6$ states [4] have shown a strong l dependence of the excitation spectra. It is attributed to multipole effects, the importance of which increases as the inner turning point of the outer electron decreases. This study has demonstrated that the two-electron "planetary" image based on their long-range dipole interaction breaks below $l\approx 7$ for $8s$. The observed induced mixing with the $5fn'l'$ series in the $8sn=13$ and $14l=6$ spectra requires that terms higher than the dipole term be considered in the multipole expansion of the anisotropic part of the e-e interaction.

A detailed and quantitative analysis of such spectra needs, of course, advanced theoretical calculations, presenting a challenging task for theorists. Recent calcu-

*Present address: Institut de Physique Nucléaire, 91406 Orsay Cedex, France.

lations using the R-matrix procedure in combination with multichannel quantum-defect theory (MQDT), including the adiabatic effects of long-range multipole interactions [5], are to be considered as a first step in this direction. On a more qualitative basis, the totality of the experimental data recorded on those ADR states with low- and high-l outer electrons (see [6], and references therein) leads to two conclusions. First, the appearance of e-e correlation effects in the spectra is unavoidably connected with strong polarization phenomena, the prediction of which would allow future studies to be performed in a more controllable manner. Second, it is therefore evident that experimental studies dealing with measurements of dipole and higher-order inner-electron polarizabilities are of immediate interest.

Polarizabilities are directly connected to second-order shifts of energy levels. Although high-l_1 core electrons with near-zero quantum defects are highly polarizable as observed in Sr [3] by using $6f$ excitation, similar $8f_{j1}nl$ ADR spectra recorded in Ba [7] with $n \approx 20$ suffered from three types of difficulty: the weaker polarizability of the Ba^+ Nf states compared to those of Sr^+ Nf due to their larger quantum defects; the $(2j_1+1)$ number of nondegenerate K components due to first-order energy corrections [2], and the feebly l-mixed initial Rydberg state in our experimental setup [8]. In this respect and in spite of their weaker polarizability (quantum defect ≈ 3.6 for Ba^+ Ns states), $Ns_{1/2}nl$ ADR investigations seem to be more appropriate for polarizability measurements and systematics since the two $K = l \pm 1/2$ components are degenerate, simplifying considerably the analysis of the data. Additionally the observed structures, are free of first-order shifts and of perturbations having their origin at fine-structure interactions.

In the present paper, we report on spectroscopic studies for high-l $Nsnl$ ADR states with $N=8$ and 9. From a quantum-defect analysis of the data, we are able to determine the Ba^+ $8s$ and $9s$ effective dipole and quadrupole polarizabilities. By combining those numbers with derived ones from $N=7$ and 10 data recorded previously [8], we analyze the evolution of the effective dipole and quadrupole polarizability versus N^* of the Ba^+ Ns core by increasing its radial extension without any penetration in the space occupied by the outer nl electron.

The following part is divided into three sections: the first, where we briefly describe our experimental procedure and the sets of measurements for the $8s$ and $9s$ inner-electron excitations; the second, where we present the parametrization of the dipole and quadrupole effective polarizabilities for the Ba^+ Ns core and the fitted values derived from our observations; and finally the third, where we compare the results of our fits with calculated static polarizabilites to show the importance of dynamical effects due to the motion of the high-l outer electron.

II. EXPERIMENTAL PROCEDURE AND $Nsnl$ ADR LEVELS FOR $N=8$ AND 9

Our apparatus and experimental procedure have been previously described [1], so here we give a brief summary and focus only on details relevant to the present study. Ground-state Ba atoms emerging from an effusive atomic beam interact with two dye laser beams in the presence of a static electric field F (1500–800 V/cm). The first laser excites the atoms to the $6s6p\ ^1P_1$ level ($\lambda_1 = 553.5$ nm) and the second ($\lambda_2 \approx 430$ nm) to a selected $6snk$ Stark state ($n = 12-15$ and $k = n-1$ to 5). The field is then turned off slowly enough for the Stark state to evolve adiabatically to the corresponding $6snl = k$ Rydberg level in zero field. Then, a third laser is fired, driving the $6s \rightarrow 8s$ ($\lambda_3 \approx 344.6$ nm) or $6s \rightarrow 9s$ ($\lambda_3 \approx 304.4$ nm) two-photon excitation of the remaining valence electron. The finally populated $Nsnl$ ADR levels are detected by monitoring the Ba^{2+} signal recorded as a function of the third laser's frequency, using a time-of-flight TOF analyzer and a tandem of microchannel plates. The Ba^{2+} ions are created in either of two ways: photoionization of excited Ba^+ levels produced by autoionization of the $Nsnl$ ADR states and direct resonant double photoionization. Evidence for this latter mechanism, frequently considered as having negligible probability, was seen in the Ba^{2+} yield vs laser intensity analysis of the $8sn = 13, 14l$ ($l \geq 10$) ADR states [9]. The third laser also photoionizes parasitic ground-state Ba^+ ions through the $8s$ or $9s$ two-photon ionic transitions, thus providing absolute frequency calibration of our Fabry-Pérot étalon's transmitted fringes, recorded simultaneously with the Ba^{2+} ion spectrum. These Ba^+ Ns lines also offer very useful markers pointing toward the expected $Nsnl$ energy-level position in the extreme case of uncorrelated highly asymmetrically excited DR states (the outer electron being at infinity).

In a previous publication [8] for $7s$ and $10s$, we have performed a detailed study of residual stray-field effects present in our apparatus (≤ 1 V/cm) at the moment that the third laser is fired. As a result for $n > 12$, in addition to the main $10snl$ excitation line corresponding to the principal $l = k$ component of the selected $6snl = k$ initial level, the spectra also exhibit weaker $10snl = k \pm 1$ transitions corresponding to adjacent $l = k \pm 1$ Stark-state degeneracy. This tray field has no effect on the final ADR state since it represents a very small perturbation compared to the normally increased electron-electron interaction due to the extension of the inner-electron spatial distribution. By the use of a very weak externally applied dc voltage (up to 5 V), we benefited from this l mixing to allow unambiguous line identification in the excited spectra by varying the initial Stark-state composition and the intensity of the corresponding $l = k$ and $k \pm 1$ resonances [8]. Having thus identified all the $Nsnl$ ADR states for $N = 8-10$, we present in Fig. 1 typical $9sn = 14l$ spectra recorded from $k = 12, 9, 8, 7$ selected Stark states. The letter k is here preferred instead of l because these spectra were recorded intentionally in l-mixing conditions at a 5-V dc voltage when firing the third laser to guarantee the presence of as many $l = k, k \pm 1, k \pm 2$ excited transitions as possible at each selected k value. In the $9snl = 6$ spectrum, not reported here, only an unstructured broad continuum signal is apparent.

We can notice in Fig. 1 that all the $9sn = 14l$ lines undergo a red shift with respect to the Ba^+ $6s \rightarrow 9s$ ionic transition. The blue-shifted broad resonance marked by

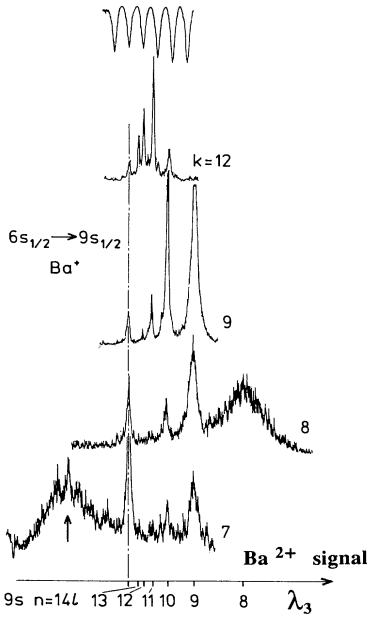

FIG. 1. Two-photon excitation spectra $6s_{1/2}nl \rightarrow 9s_{1/2}nl$ from different initially selected $6sn = 14k$ levels with $k = 12$, 9,8, and 7. These spectra are calibrated to the two-photon $6s_{1/2} \rightarrow 9s_{1/2}$ Ba^+ transition. The positions of the $9sn = 14l$ resonance lines are identified by their l values on the bottom energy scale. The Fabry-Pérot fringe spacing is 4 cm^{-1}. In the $k = 7$ spectrum, the arrow indicates the $9s_{1/2}n + 1 = 15l = 7$ resonance recorded from the $6sn = 14k = 7$ level. The corresponding $9s_{1/2}n = 14l = 7$ resonances is toward the low-energy side of the $k = 7$ spectrum and out of the presented scanned wavelength range with the third laser λ_3.

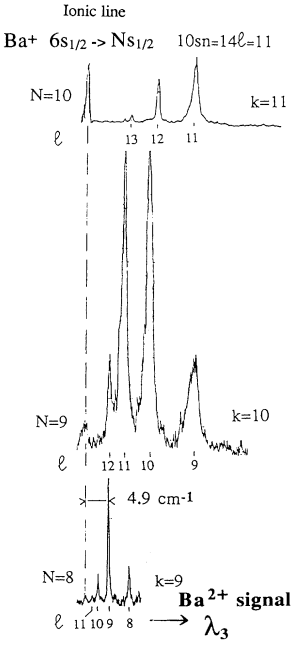

FIG. 2. Two-photon excitation spectra $6s_{1/2}n = 14l \rightarrow Ns_{1/2}n = 14l$ with $N = 8-10$ from different initially selected $6sn = 14k$ levels. These spectra are calibrated to the two-photon $6s_{1/2} \rightarrow Ns_{1/2}$ Ba^+ transitions. Positions of the $Nsn = 14l$ resonance lines are marked by the indicated l values on the bottom of each spectrum.

an arrow in the spectrum labeled $k = 7$ represents an exception. It is identified as the transition to the $9sn = 15l = 7$ level, which appears in the $n = 14$ recording because its quantum defect approaches unity. A similar broad resonance for $9sn = 14l = 7$ is observed in the $n = 13$, $k = 7$ spectrum, which is not represented in Fig. 1. This large quantum defect, together with the broad $9snl = 8,7$ linewidths, point out that inner-electron penetration of the external electron induces strong mixing with available continua for those states. Figure 2 shows the increase of these red shifts at fixed l values for the $Nsn = 14l$ ADR states when the inner Ns electron is radially extended from $N = 8-10$ (for example, follow in Fig. 2 the increasing value of the shifts for the $8sn = 14l = 11$, $9sn = 14l = 11$, and $10sn = 14l = 11$ resonances). However, due to the absence of perturbers in these energy ranges, the spectra present a simple single-line character. This is not the case for $8snl = 7$ and especially $8snl = 6$ states, which were recently found to be heavily mixed by induced multipole coupling with $5f_{5/2,7/2}n'l'$ series, resulting in a very complex and extended spectra [4]. The above-mentioned observations forced us to restrict the following polarizability determination to $n = 13-15l \geq 8$ for $8s$, $n = 12-15l \geq 9$ for $9s$, and $n = 13-15l \geq 10$ for $10s$ excitations, where good spatial separation between the two electrons leads to negligible exchange effects. Mixing with $5f_{7/2}n'l'$ states appeared also for $8sn = 15l = 8$ and $8sn = 12l \leq 10$ spectra, which were excluded from our parameterization procedure. We report in Tables I and II the excitation energy of the identified resonances between the chosen $6snl$ initial states and the final $8snl$ and $9snl$ ADR levels. By the use of two-photon transition for the inner-electron excitation, tabulated values are twice the calibrated photon energy of the third uv laser, which is obtained by frequency doubling the dye beam.

III. THEORETICAL CONSIDERATIONS AND DATA PROCESSING OF THE $Nsnl$ ADR LEVELS

The core-polarization theory applied to hydrogenlike atoms [10] is not new and it is well known that quantum defects for low-l penetrating orbits are of a different nature from those of nonpenetrating high-l orbits. In the

TABLE I. Energy (cm^{-1}) of the two-photon transition corresponding to the $6snl \rightarrow 8snl$ resonance.

l	$n = 13$	$n = 14$	$n = 15$
7	perturbed	58 008.38(10)	58 011.64(65)
8	58 014.13(15)	58 016.07(5)	perturbed
9	58 019.26(7)	58 020.28(10)	58 021.28(2)
10	58 021.84(5)	58 022.40(15)	58 022.07(7)
11	58 023.22(5)	58 023.53(5)	58 023.84(6)
12	blended	58 024.15(10)	58 024.37(4)
13			58 024.67(6)

TABLE II. Energy (cm^{-1}) of the two-photon transition $6snl \rightarrow 9snl$ resonances.

l	$n=12$	$n=13$	$n=14$	$n=15$
		$6snl \rightarrow 9snl$ resonance		
8	65 632.8 (8)	65 642.4 (10)	65 649.4 (3)	65 654.2 (9)
9	65 656.4 (2)	65 661.2 (3)	65 665.1 (2)	65 668.4 (2)
10	65 667.6 (2)	65 670.2 (2)	65 672.4 (2)	65 674.4 (1)
11	65 673.98 (5)	65 675.6 (1)	65 676.6 (1)	65 677.7 (1)
12		65 678.5 (2)	65 679.2 (2)	65 679.9 (1)
13			65 680.7 (1)	65 681.1 (1)
		$6snl \rightarrow 9s(n+1)l$ resonance		
7	65 713.4 (30)	65 705.4 (20)	65 693.4 (30)	65 700.4 (20)

latter case, the quantum defect is determined almost entirely by the polarization of the atomic core in the field of the outer electron. Such information has previously been deduced from properties of high-l Rydberg states in alkali-metal atoms [11] and alkalilike ionized atoms with a closed-shell core [10,12,13]. In general, because of the much higher speed of the residual core electrons compared to the outer electrons, the latter can be regarded as stationary, producing a polarizing field constant in time. This approximation constitutes the basis of the adiabatic (or static) model [14]. However, this description is not entirely satisfactory for moderate l orbits in alkali-metal atoms [11] or systems with partially filled cores [15], such as alkaline-earth atoms [16]. There the movement of the outer electron cannot be neglected (nonadiabatic model) and the description of the core deformatoin induced is complicated by this dynamical effect.

For alkaline-earth-atom high-l ADR states, the outer electron does not penetrate appreciably the inner electron, which with the residual doubly charged core constitutes a singly charged excited ion. In this case, the quantum defect essentially arises from long-range electron-electron interaction. It is particularly interesting in the core-polarization theory to examine the validity of the adiabatic approximation and to identify the l orbits where nonadiabatic effects cannot be neglected. This sudden change in the character of the two-electron interaction is reminiscent of recent investigations in Sr [3]. There, the nature of the change in the spectra vs the principal quantum number n of the outer electron was explained by the transition from a permanent to an induced dipole formed by the inner electron and the residual ionic core.

A. Dipole and quadrupole polarization formulas

The second-order energy-level correction for a spherically symmetric inner-Ns-electron core (free of first-order corrections) is given by the following formula [17] in atomic units:

$$\Delta E_{nl}^{Ns} = -\tfrac{1}{2}\alpha_d[y_0^{(1)}\langle r^{-4}\rangle_{nl} + y_2^{(1)}\langle r^{-6}\rangle_{nl}] - \tfrac{1}{2}\alpha_q[y_0^{(2)}\langle r^{6}\rangle_{nl} + y_2^{(2)}\langle r^{-8}\rangle_{nl}] , \quad (1)$$

where the nonadiabatic effects are explicitly taken into account. ΔE_{nl}^{Ns} is the energy-level shift from the uncorrelated hydrogenic position $-1/(2n^2)$ with respect to the $Nsnl$ series limit and $\langle r^{-4}\rangle_{nl}$, $\langle r^{-6}\rangle_{nl}$, $\langle r^{-8}\rangle_{nl}$ are expectation values for the inverse fourth, sixth, and eighth powers of the outer-electron radius. The α_d and α_q coefficients are the static dipole and quadrupole polarizabilities for the Ba^+ Ns levels, respectively given by

$$\alpha_q = \frac{2}{2q+1}\sum_{K\neq 0}\frac{|\langle 0|r|K\rangle|}{\varepsilon_K - \varepsilon_0} \quad \text{with } q=1,2 , \quad (2)$$

where $\varepsilon_{K,0}$ are the energy-level positions and $\alpha_d=\alpha_1$ and $\alpha_q=\alpha_2$.

The $y_i^{(q)}$ parameters described the modifications induced by nonadiabatic effects. Electron exchange is neglected. Equation (1) for $y_0^{(1)}\rightarrow 1$ and $y_2^{(1)}\rightarrow 0$ is reduced to the customary adiabatic formula

$$\Delta E_{nl}^{Ns} = -\tfrac{1}{2}[\alpha_d\langle r^{-4}\rangle_{nl} + \alpha_q\langle r^{-6}\rangle_{nl}] . \quad (3)$$

In fact, the parameters $y_i^{(q)}$, which are expected to be slowly varying functions of n and l (for a given N), cannot be extracted from an energy-level fit parametrization. A formula similar to (3) by neglecting the $y_2^{(2)}\langle r^{-8}\rangle_{nl}$ term in (1) yields only l-averaged effective dipole α_d' and quadrupole α_q' polarizabilities, including indirectly the nonadiabatic effects. Then, these effective α_d' and α_q' polarizabilities are connected with those given by (2) using the calculated relations $\alpha_d' = y_0^{(1)}\alpha_d$ and $\alpha_q' = y_2^{(1)}\alpha_d + y_0^{(2)}\alpha_q$.

The parameter $y_0^{(1)}$ has been found to be a smooth function of n for bound alkali-metal [11] and alkaline-earth-atom high-l states [16]. Unfortunately, the evaluation of $y_0^{(2)}$ and $y_2^{(1)}$ as their extrapolation for different values of n, l, and N is not simple and represents a formidable task in itself [11]. However, for a semiempirical outer-electron wave-function determination, it is preferable to know these effective polarizabilities since they automatically include nonadiabatic effects that are not easy to estimate theoretically [18].

Since the dipole e-e interaction term is by far the dominant term, the magnitude and N^* scaling of the corresponding α_d' polarizability is not expected to be severely affected by nonadiabatic effects. On the contrary, α_q' polarizabilites are extremely sensitive to perturbations and

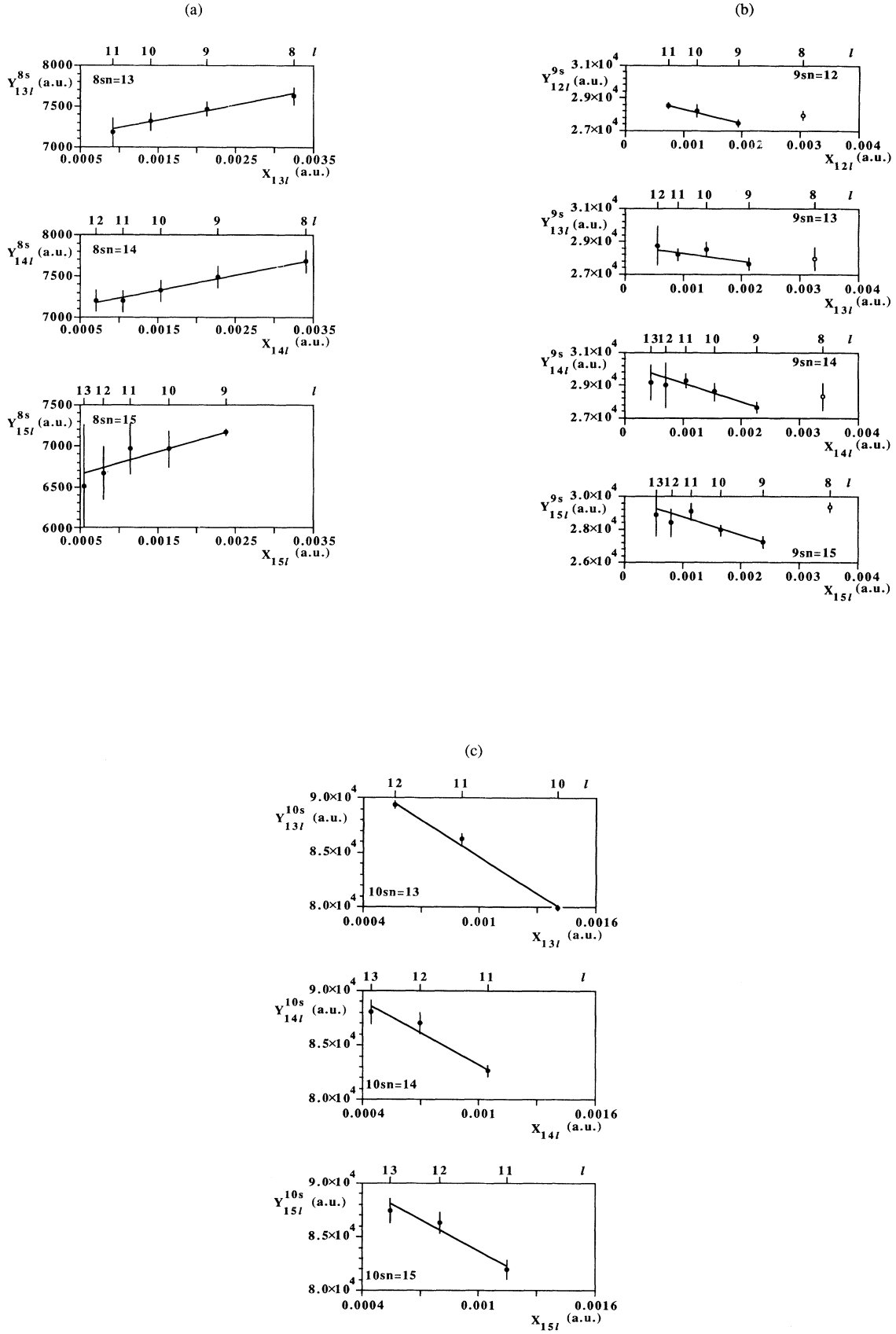

FIG. 3. Y vs X graphs for $Nsnl$ double Rydberg states: (a) $N=8$, (b) $N=9$, and (c) $N=10$.

the relation between α'_q and static α_d, α_q values is not as simple as the one for the dipole polarizability.

B. Data parametrization of the observed *Nsnl* ADR levels for $N=7-10$

The energy shift of the line corresponding to a $6snl \rightarrow Nsnl$ transition from the Ba^+ $6s \rightarrow Ns$ two-photon transition appearing in our data (see Fig. 1 and 2) is equal to $\Delta E_{nl}^{Ns} - \Delta E_{nl}^{6s}$, and so calculation of ΔE_{nl}^{Ns} requires the knowledge of ΔE_{nl}^{6s} of the initial level. We determine the latter by applying formula (3) and using experimentally derived Ba^+ $6s$ dipole and quadrupole polarizabilities [16]. The nonadiabatic $y_i^{(q)}$ parameters for $l \geq 8$ and $n=12-15$ are unknown, but they should cause insignificant changes to the actual Ba^+ ground-state polarizability magnitudes for such high-l states, as judged by their calculated trend for $18 \leq n \leq 23$ and $4 \leq l \leq 7$ [16]. Hence we neglect nonadiabatic corrections and use static polarizabilities instead. The calculated $6snl$ $l \geq 8$ energy-level depressions are as a rule less than our uv-λ_3 laser linewidth [≈ 3.5 GHz full width at half maximum (FWHM)] and in general far smaller than the experimentally measured energy separation for $N > 6$ s-core electron excitation. This is not surprising since for high-l $6snl$ states the e-e correlation effects are far smaller. As a result, the uncertainties for the ΔE_{nl}^{Ns} values originate from the energy measurement of the $6snl \rightarrow Nsnl$ transitions. Those used in our fits are reported in Tables I and II for $8s$ and $9s$ excitations and in Tables I and III of Ref. [8] for $7s$ and $10s$ excitations. Most of them are limited by our laser instrumental resolution, but larger errors are principally due to accidental blending for high-l levels or large autoionization widths for the lowest l ones.

In order to fit our measured data, formula (3) is used in the form $Y=\alpha'_d+\alpha'_q X$ with $Y=-2\Delta E_{nl}^{Ns}/\langle r^{-4}\rangle_{nl}$ and $X=\langle r^{-6}\rangle_{nl}/\langle r^{-4}\rangle_{nl}$ in a.u. Hydrogenic values are used for the radial matrix elements. Thus α'_d and α'_q effective polarizabilities are the intercept and slope, respectively, of a Y vs X graph, expected to be a straight line. To fit the two parameters, only a set of different l measurements for the same n value is required. Any other set of l measurements for different n is fitted independently and increases the accuracy of α'_d and α'_q determinations if it is free of strong perturbations.

In Fig. 3(a), we show the graphs for $8snl$ states with $n=13$ $l=8-11$, $n=14$ $l=8-12$, and $n=15$ $l=9-13$. We can see that for $n=13$ and 14, the fitted α'_d values are practically the same and within small uncertainties. Scattering of the points together with their larger uncertainties means that the $n=15$ fit reveals a smaller intercept that deviates from the $n=13$ and 14 values. This can be attributed to the presence of perturbers belonging to series converging to higher thresholds than $8s$ [5] and/or the high density of $5f_{7/2}n'l'$ states in the neighborhood of the $8sn=15l$ states [4]. In this case, the simple perturbative model leading to formula (3) is not well adapted to reproduce accurately such mixings. For this reason, the Ba^+ $8s$ effective dipole polarizability given in Table III is determined by averaging the fitted values from only the $n=13$ and 14 data.

In Fig. 3(b), we present the graphs for $9snl$ states with $n=12$ $l=8-11$, $n=13$ $l=8-12$, $n=14$ $l=8-13$, and $n=15$ $l=8-13$. It can be seen that the lowest l points (usually ≈ 8) deviate from the fitted straight lines determined by the higher-l points. This deviation is due to penetration effects in the inner electron [supported also by the autoionization width of the lines (see Fig. 1)] not taken into account by formula (3). Consequently, the applicability of our parametrization for the Ba^+ $9s$ core state is limited to $l \geq 9$. Unlike the $8s$ data, all the fits give consistent α'_d values within their uncertainties, in spite of the small scatter of few $l > 8$ points. This is to be expected because the density of possible perturbers belonging to higher excited core states increases.

Previously, Ba^+ $7s$ and $10s$ effective dipole and quadrupole polarizabilities have been determined [8] by the use of a simpler formula compared to (3) valid only for $l \approx n$. In order to present a unified treatment for all the Ns excited core investigated, we repeat the procedure presented above for $7s$ and $10s$ data using (3). The plots for $N=7$ reveal a strong scattering for the highest l points (see Fig. 3 in Ref. [8]) attributed to the lack of instrumental resolution due to the stray-field effect previously mentioned, which prevents resolution of the $l=k$ and $k\pm 1$ lines. To determine at least an intercept for the $N=7$ graphs (which are not presented here), we use the lowest l measurements belonging to completely resolved lines ($l \geq 6$) that might not be completely free of possible penetration effects. In Fig. 3(c), we report the graphs for $10snl$ states with $n=13$ $l=10-12$, $n=14$ $l=11-13$, and $n=15$ $l=11-13$. For the $n=13$ graph, we use the $l=10$ level, although its width is indicating substantial overlapping of the two excited electrons. When this point is ignored, the resulting slope and intercept match more closely those of the two $n=14$ and 15 graphs.

TABLE III. Effective α'_d dipole polarizabilities for Ba^+ Ns state (a_0^3).

n \ N	7	8	9	10
12	$1.06(3)\times 10^3$ [a]		$2.919(8)\times 10^4$	
13	$1.25(9)\times 10^3$	$7.06(4)10^3$	$2.88(5)\times 10^4$	$9.58(8)\times 10^4$
14	$1.21(4)\times 10^3$	$7.04(3)10^3$	$3.03(3)\times 10^4$	$9.29(18)\times 10^4$
15	$1.29(4)\times 10^3$	$6.52(9)10^3$ [a]	$2.98(5)\times 10^4$	$9.3(2)\times 10^4$
		n-averaged value		
α'_d	$1.25(5)10^3$	$7.05(4)10^3$	$2.95(4)10^4$	$9.39(15)10^4$

[a]Values not taken in account for the average determination.

We can notice immediately by comparing the fitted straight lines in the graphs of Figs. 3(a)–3(c) that their intercept and slopes are roughly identical at fixed values of N and different values of n but that their slopes are strongly dependent of N. Particularly the slope's sign, which is positive for $N=8$, becomes clearly negative for the $N=9$ and 10 fitted straight lines.

1. *Effective dipole polarizabilities*

The intercepts of all the fitted straight lines in the Y vs X graphs with their n-averaged values are assembled in Table III. We can notice that the $7s$ α'_d value for $n=12$, which is derived from the lowest l measurements, shows a stronger dependence on nonadiabatic effects than those derived from the $n=13-15$ fits; hence the $n=12$ value has not been used in the averaged determination. For these low-l values, closed-channel mixing can be also present, as evidenced by spectroscopy of the $7sng$ states [19], which revealed serious perturbations confirmed by theoretical calculations [20]. Consequently, the relative error for the $7s$ α'_d polarizability is the largest of our determined values.

2. *Effective quadrupole polarizabilities*

Table IV assembles the fitted slopes and their uncertainty extracted from the Y vs X graphs, which correspond to the effective α'_q quadrupole polarizabilites. We can notice that the scatter of the $7sn=12$, $8sn=15$, and $9sn=13$ values is larger than the other determinations due to the considerations presented above (lack of resolution for $7s$ and possible perturbers for $8s$ and $9s$). The change in $N=9$ and 10 α'_q signs is discussed in more detail below and attributed to outer-electron dynamical effects acting on a Ba^+ core of increased size. It also prevents the study of systematics for α'_q polarizabilities.

IV. COMPARISON BETWEEN EFFECTIVE AND CALCULATED STATIC POLARIZABILITIES

Inspection of definition (2) for $q=1$ reveals the expected dipole polarizability scaling law with the effective N^* quantum number. For the Ns members, only the few $N'p$ states energetically closest to the one under study contribute $\simeq 90\%$ or more to the summation in (2). They also determine the sign of α_d. For this reason we expect α_d to follow an N^{*7} power dependence if N^* is high enough to ensure a Rydberg character of the states. In this case, the squared matrix elements in the numerator scale as N^{*4} and energy differences in the denominator as N^{*-3}.

In order to take into account the valence character of the Ns and Np states for $N \leq 7$, we have performed calculations of the static dipole polarizabilities using matrix elements provided by two sources (A and B), and the results are shown in Table V. For A, the static values are calculated using matrix elements provided by a method similar to the one described in Ref. [18]. In the $Z=2$ Coulomb potential, dipole and quadrupole polarization terms were added, and we have used corresponding effective polarizabilities of the Ba^{2+} ion taken from the analysis of the Ba^+ Ng series [12]. We have used a cutoff radius of $1.85a_0$ that is the same as in Ref. [18]. For B, the matrix elements were calculated using a model potential [21]. In both calculations, experimental Ns and spin-orbit averaged $N'p$ level energies have been used with $N' \leq 12$. As we can see, the calculations show perfect agreement for $N=6$, which is closer to the $144.1a_0^3$ Hartree-Slater result [22] than the $122.6a_0^3$ calculated in the Coulomb approximation [16]. For low N, the agreement is satisfactory but there is an increasing deviation for $N \geq 9$. If we compare our fitted effective values in Table III and the calculated static ones given in Table V, the overall agreement for $N>6$ is very good within 10% except for the set A, $N=10$ value.

The N^* power dependence of the calculated static dipolar values is given in Table V and is somewhat lower than the above derived value involving states with pronounced Rydberg character. Of course, by increasing N, the power dependence would probably evolve gradually from $\approx 6.5-7$. If nonadiabatic effects were not important, an experimentally derived N^* power dependence should coincide with the one derived by the calculated static polarizabilities.

Figure 4 shows the log-log plot of our fitted α'_d values with respect to N^* for $N \geq 7$. Fitting the points weighted by their uncertainties, we determine an $N^{*6.9(1)}$ power dependence. By comparing this result to the $N^{*6.5}$ power dependence of the calculated dipole polarizabilities, we can conclude that the disagreement should be considered as a signature of nonadiabatic effect and not as a confirmation of the N^{*7} scaling law expected for high-N Rydberg states. Even more, this experimentally derived

TABLE IV. Effective α'_q quadrupole polarizabilities for Ba^+ Ns states (a_0^5).

n \ N	7	8	9	10
12	$9.5(11)\times 10^4$ [a]		$-0.88(6)\times 10^6$	
13	$2.1(1.7)\times 10^4$	$1.80(18)\times 10^5$	$-0.52(33)\times 10^6$ [a]	$-1.12(6)\times 10^7$
14	$1.9(5)\times 10^4$	$1.89(16)\times 10^5$	$-1.15(17)\times 10^6$	$-0.97(20)\times 10^7$
15	$1.2(3)\times 10^4$	$2.72(40)\times 10^5$ [a]	$-1.09(28)\times 10^6$	$-0.95(22)\times 10^7$
		n-averaged value		
α'_q	$1.7(8)\times 10^4$	$1.84(17)\times 10^5$	$-1.04(17)\times 10^6$	$-1.01(16)\times 10^7$

[a]Values not taken in account for the average determination.

TABLE V. Calculated static α_d dipole polarizabilities for Ba^+ Ns states (a_0^3).

N	A	B
6	139.2	139.8
7	1411	1457
8	7504	7870
9	28332	30027
10	85437	91382
	Fitted N^* power dependence	
for $N \geq 6$	6.35	6.41
$N > 6$	6.42	6.47

TABLE VI. Calculated static α_q quadrupole polarizabilities for Ba^+ Ns states (a_0^5).

N	A	B
6	3 701	4 536
7	165 627	169 728
8	6 083 476	6 133 552
9	26 591 948	26 840 639
10	167 785 350	169 397 750
	Fitted N^* power dependence	
for $n \geq 6$	10.69	10.52

law can be used to extrapolate effective dipole polarizabilities for $N > 10$ for predicting energy-level positions of high $Nsnl$ DR states and the relative importance of dielectronic correlation effects.

For example, we know that a dipole polarizability of $\approx 5 \times 10^5$ a_0^3 for Sr^+ $7f$ leads to clearly observable spectral signatures of long-range correlation in the overlap structure of Sr $7fnl$ excitation [3]. Using our $N^{*6.9}$ fitted power law, we can predict that for Ba^+ Ns states we will reach the same dipole polarizability magnitude for $N \approx 12$. Of course, verification of this prediction in the Ba $12snl$ ADR state analysis, based on single-line excitation spectra as in the present study for $N = 7-10$, would require n and l of the outer electron to be appropriately increased in order to avoid its inner-electron penetration and closed-channel mixing induced by short-range effects [4]. This situation is unfortunately inaccessible at the moment because the adiabaticity criterion in the Stark switching technique will not be met for $n > 15$.

Calculated static quadrupole α_q polarizabilities using the above described methods are given in Table VI. No direct comparison of these values with the fitted effective ones can be made because of differences by orders of magnitude and positive signs exhibited by all of them. This confirms that the relation between effective and static values for the quadrupole polarizabilities is not as simple as the dipole polarizability, a point already mentioned above. Nonadiabatic corrections to the polarization interaction are known to be small for alkali-metal and alkali-metal-like systems [17,23,24]; on the contrary, in two-electron systems with the inner valence electron not excited and the outer in a Rydberg state, dynamical effects are expected to be substantial [16]. Even more, when the inner electron is strongly excited, we expect a considerable enhancement of their importance that should scale with its increasing radial size. Using a classical calculation, we found that the Ba^+ $10s$ size is 14 times larger than for $6s$, so we expect a strong dependence of α_q' on N. We should mention that the observed strong dependence characterized by the change of sign for $N \geq 9$ cannot be attributed to penetration effects, since similar classical calculations show that the inner turning point of the nl outer electron is always larger than the Ns core size. Moreover, this negative sign is consistent with an increasing importance of nonadiabatic effects, since these are always raising the energy levels towards the corresponding hydrogenic positions [23].

To get a feeling about the effects of the smaller magnitude and sign change of α_q' quadrupole polarizability, we can write the effective potential $V_{\text{eff}}(r)$ seen by the outer nl electron:

$$V_{\text{eff}}(r) = -\frac{1}{r} + \frac{l(l+1)}{2r^2} - \frac{\alpha_d}{2r^4} f_d - \frac{\alpha_q}{2r^6} f_q \ , \tag{4}$$

where f_d and f_q are appropriate cutoff functions [18]. The cutoff radius r_c used is the Ns outer turning point.

If the static dipolar and quadrupolar values (adiabatic model) are replaced by our α_d' and α_q' values, to take into account nonadiabatic effects, this leads to a noticeably less attractive potential shown in Fig. 5 for the $10sl = 11$

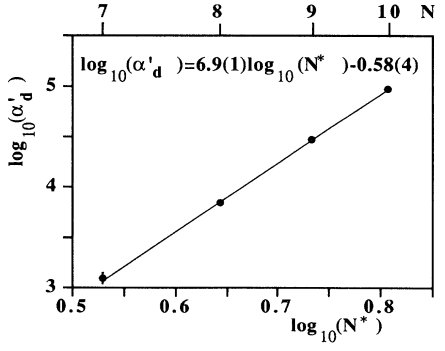

FIG. 4. Log-log plot of the effective dipolar polarizabilities for Ba^+ Ns vs the core principal quantum number N^*.

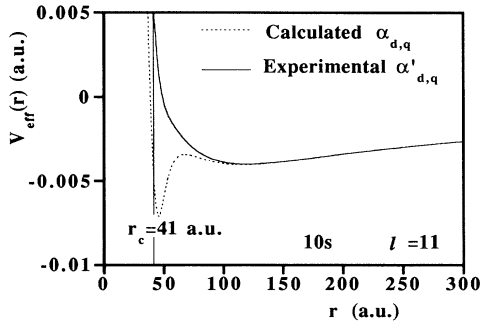

FIG. 5. Calculated $V_{\text{eff}}(r)$ potential seen by the outer $l = 11$ electron for the $10s$ ADR state: comparison between the theoretical $\alpha_{d,q}$ static model and our experimental effective $\alpha_{d,q}'$ parametrization.

state. It is interesting to note here the minor contribution introduced by the small differences between α_d' and α_d (see their comparison above). By contrast, both the reduced magnitude and reversed sign of α_q' are dominating the changes there by indicating the importance of dynamical effects between the two electrons. It is evident that a less attractive potential would lead to a modification of the short-range two-electron interaction, which cannot be reproduced by an adiabatic theory. It proves that dynamical effects on the inner Ns electron caused by the motion of the outer electron cannot be neglected, even if the latter is in a high-l orbital.

V. CONCLUSION

We have presented experimental measurements of energy-level positions for Ba $8snl$ and $9snl$ high-l states. The studied spectra exhibit a simple single-line picture and thus they are not significantly affected by closed-channel mixings previously revealed for low-l $8snl$ states [4]. This enabled us to parametrize our data as well as previously reported for $Nsnl$ states with $N=7$ and 10 [8] using a simple polarization formula. Effective dipole polarizabilities for Ba^+ Ns states, $N=7$–10 were determined and found to follow a $N^{*6.9(1)}$ power law. Even if this result is very close to the expected N^{*7} behavior for states with pronounced Rydberg character, it should be considered only as an indication of nonadiabatic effects since calculated static polarizabilities present a lower power dependence. However, the dipole polarizabilities are not very sensitive to these effects and the overall agreement between experimental effective and theoretical static values justifies that weak channel mixings and small core penetration are not able to mask the characteristics and strength of the dominant long-range dipole interaction. This experimentally derived power law can be used to extrapolate Ba^+ Ns effective dipole polarizabilities for $N>10$ and $Nsnl$ ADR states where long-range dipolar effects on the wave function of the outer electron should be observable as an ICE envelope modification. Effective quadrupole polarizabilities show a sudden change of sign for $N>9$, which can be attributed mainly to dynamical nonadiabatic effects by simple classical considerations. It demonstrates the importance of the core electron orbital size in the spectral properties of asymmetrical double Rydberg states even in the case of a nonpenetrating outer electron. It gives evidence of the dynamical nature of their correlation in planetary situations.

ACKNOWLEDGMENTS

It is a pleasure to acknowledge M. Aymar for providing Ba^+ calculated radial matrix elements by the model potential method, and M.S. Child for careful reading of the manuscript and to thank G. Hubbard for her technical assistance. The Laboratoire Aimé Coton is associated with the Université Paris-Sud.

[1] L. Pruvost, P. Camus, J-M. Lecomte, C. R. Mahon, and P. Pillet, J. Phys. B **24**, 4723 (1991).
[2] P. Camus, J-M. Lecomte, C. R. Mahon, P. Pillet, and L. Pruvost, J. Phys. II (France) **2**, 715 (1992).
[3] U. Eichmann, V. Lange, and W. Sandner, Phys. Rev. Lett. **68**, 21 (1992).
[4] P. Camus, S. Cohen, L. Pruvost, and A. Bolovinos, Phys. Rev. A **48**, R9 (1993).
[5] R. P. Wood and C. H. Greene, Phys. Rev. A **49**, 1029 (1993).
[6] P. Camus, Phys. Scr. **T51**, 20 (1994).
[7] P. Camus, J-M. Lecomte, C. R. Mahon, P. Pillet, and L. Pruvost, *Laser Spectroscopy TENICOLS'91* Font-Romeu, edited by M. Ducloy, E. Giacobino, and G. Camy (World Scientific, Singapore, 1992), p. 431.
[8] P. Camus, C. R. Mahon, and L. Pruvost J. Phys. B **26**, 221 (1993).
[9] S. Cohen, P. Camus, and A. Bolovinos, J. Phys. B **26**, 3783 (1993).
[10] K. Bockasten, Phys. Rev. **102**, 729 (1956); see also B. Edlèn, in *Atomic Spectra,* edited by S. Flügge, Hanbuch der Physik, Vol. 27 (Springer, Berlin, 1964), pp. 123–129 and 185–191, and references therein.
[11] R. R. Freeman and D. Kleppner, Phys. Rev. A **14**, 1614 (1976), and references therein.
[12] R. R. Jones and T. F. Gallagher, J. Opt. Soc. Am B **6**, 1467 (1989).
[13] V. Lange, M. A. Khan, U. Eichmann, and W. Sandner, Z. Phys. D **18**, 319 (1991).
[14] J. E. Mayer and M. Goeppert Mayer, Phys. Rev. **43**, 605 (1933).
[15] J. H. Van Vleck and N. G. Whitelaw, Phys. Rev. **44**, 551 (1933).
[16] T. F. Gallagher, R. Kachru, and N. H. Tran, Phys. Rev. A **26**, 2611 (1982).
[17] A. G. Vaidyanathan and P. Shorer, Phys. Rev. A **25**, 3108 (1982).
[18] M. Poirier, Z. Phys. D **25**, 117 (1993).
[19] X. Wang and W. E. Cooke, Phys. Rev. A **47**, 1778 (1993).
[20] E. Luc-Koenig, J-M. Lecomte, and M. Aymar, J. Phys. B **27**, 699 (1994).
[21] M. Aymar, J. Phys. B **23**, 2697 (1990).
[22] L. J. Curtis, P. S. Ramanujam, and C. E. Theodosiou, Phys. Rev. A **28**, 1151 (1983).
[23] H. Eissa and U. Öpik, Proc. Phys. Soc. London **92**, 556 (1967).
[24] U. Öpik, Proc. Phys. Soc. London **92**, 566 (1967).